

Three-Dimensionally Printed Micro-electromechanical Switches

Yongwoo Lee,^{†,‡} Jungmin Han,^{†,‡} Bongsik Choi,[†] Jinsu Yoon,[†] Jinhee Park,[†] Yeamin Kim,[†] Jieun Lee,[†] Dae Hwan Kim,[†] Dong Myong Kim,[†] Meehyun Lim,[‡] Min-Ho Kang,[§] Sungho Kim,^{*,||} and Sung-Jin Choi^{*,†,§}

[†]School of Electrical Engineering, Kookmin University, Seoul 02707, Korea

[‡]Mechatronics R&D Center, Samsung Electronics, Hwaseong, Gyeonggi-do 18448, Korea

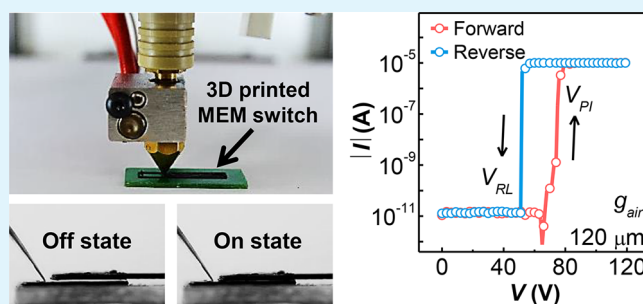
[§]Department of Nano-process, National Nanofab Center (NNFC), Daejeon 34141, Korea

^{||}Department of Electrical Engineering, Sejong University, Seoul 05006, Korea

Supporting Information

ABSTRACT: Three-dimensional (3D) printers have attracted considerable attention from both industry and academia and especially in recent years because of their ability to overcome the limitations of two-dimensional (2D) processes and to enable large-scale facile integration techniques. With 3D printing technologies, complex structures can be created using only a computer-aided design file as a reference; consequently, complex shapes can be manufactured in a single step with little dependence on manufacturer technologies. In this work, we provide a first demonstration of the facile and time-saving 3D printing of two-terminal micro-electromechanical (MEM) switches. Two widely used thermoplastic materials were used to form 3D-printed MEM switches; freely suspended and fixed electrodes were printed from conductive polylactic acid, and a water-soluble sacrificial layer for air-gap formation was printed from poly(vinyl alcohol). Our 3D-printed MEM switches exhibit excellent electromechanical properties, with abrupt switching characteristics and an excellent on/off current ratio value exceeding 10^6 . Therefore, we believe that our study makes an innovative contribution with implications for the development of a broader range of 3D printer applications (e.g., the manufacturing of various MEM devices and sensors), and the work highlights a uniquely attractive path toward the realization of 3D-printed electronics.

KEYWORDS: 3D printer, MEMS, switches, thermoplastic, water-soluble



INTRODUCTION

Three-dimensional (3D) printing can overcome general problems arising from two-dimensional (2D) processes; hence, 3D printing technologies have recently attracted considerable attention from both academia and industry for their potential applications to various fields such as aerospace, automotive, medicine, and semiconductor engineering.^{1–7} This family of manufacturing technologies enables the reliable and accurate fabrication of structures of a broad range of sizes (from the sub-micrometer scale to several meters) with complex 3D features. In particular, 3D printing is easy to use, is cost-effective, and is freely adaptable to use on a wide range of compatible materials (e.g., metals, polymers, and ceramics) to produce desired structures.^{8–15} Furthermore, nontechnical users can easily produce complex products either independently or upon request using 3D printers. In particular, by means of computer-aided design (CAD) files, various complex products such as electronic devices can be fabricated by merely sending necessary files to the 3D printer software.^{4,6,8,16–19}

Micro-electromechanical (MEM) switches have received widespread attention as promising candidates for surpassing

the limitations of currently complementary metal-oxide-semiconductor (CMOS) technologies and at present are also essential components of the circuit architectures of various MEM systems.^{20–24} MEM switches can be fabricated without semiconducting materials because they can be operated through the electrostatic actuation of a freely suspended electrode rather than through the modulation of the conductivity of a semiconducting channel. Thus, MEM switches ensure lower insertion losses and consume less power than switches based on conventional CMOS technologies such as field-effect transistors or diodes.^{21,25–27} However, as MEM switches are generally composed of complex 3D structures with suspended electrodes, they are inefficient to produce via 2D processes. In recent years, to address limitations arising from difficulties associated with fabricating MEM switches, low-cost MEM switches fabricated via inkjet printing have been reported.^{28–30} Nevertheless, complex processing

Received: January 28, 2018

Accepted: April 24, 2018

Published: April 24, 2018

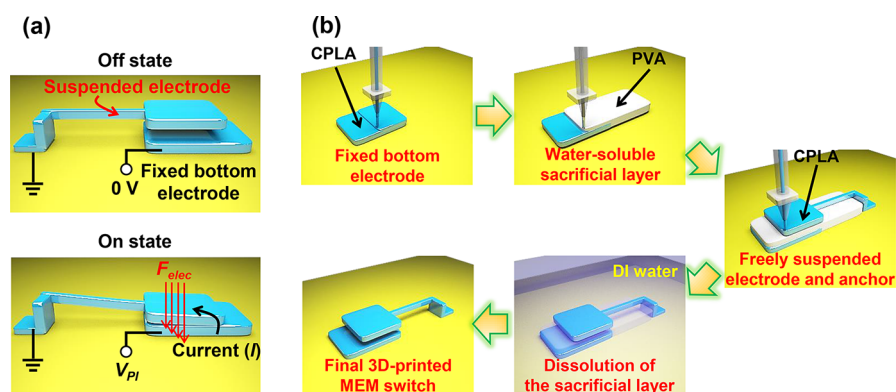


Figure 1. (a) Schematic illustrations of a 3D-printed two-terminal MEM switch in the nonconducting off state and in the conducting on state. The MEM switch exhibits a pull-in phenomenon because of the electrostatic force acting on the suspended electrode when voltage is applied to the fixed bottom electrode. (b) Process flow for the fabrication of a 3D-printed two-terminal MEM switch. First, a CPLA layer was printed to form a fixed bottom electrode. A PVA layer was then printed on the CPLA as a water-soluble sacrificial layer. Then, another layer of CPLA was printed to form a freely suspended electrode with a hammerhead structure. Finally, the PVA layer was dissolved in DI water to achieve the mechanical separation of the electrodes, yielding the final 3D-printed two-terminal MEM switch.

issues still remain (e.g., the need for separate steps for sintering, annealing, and contact electrode formation), thus resulting in low levels of throughput. However, a 3D printer can simultaneously make adjustments in three directions; hence, with use of a 3D printer, MEM switches can be fabricated without the expensive infrastructure, such as sterile rooms, photolithography equipment, and masks, required for the conventional manufacturing of MEM switches. Therefore, 3D-printed MEM switches are expected to save process time and to enable manufacturing with high throughput and at low cost.

In this paper we illustrate the fabrication of two-terminal MEM switches using a commercially available 3D printer. Two thermoplastic materials, conductive polylactic acid (CPLA) and poly(vinyl alcohol) (PVA), were used for the fabrication of 3D-printed MEM switches. Our proposed MEM switch design is composed of a two-terminal configuration consisting of a freely suspended electrode and a fixed bottom electrode; both electrodes were 3D-printed using CPLA. Mechanical separation between the electrodes was achieved by dissolving a sacrificial layer 3D-printed via PVA in water;^{31–34} this fully prevented a leakage current from forming under the nonconducting “off state”. When we applied an electrical bias between the freely suspended electrode and fixed bottom electrode, the suspended electrode collapsed toward the bottom electrode, establishing mechanical contact and creating a current path under the conducting “on state”. Our 3D-printed MEM switches exhibit excellent electromechanical properties such as abrupt switching and a high on/off current ratio. Although these two-terminal MEM switches are not appropriate for high-power radio frequency applications because of their self-actuation, they can be applied in cross-bar memory devices or transformable building blocks. Our results are expected to make an innovative contribution to the field of MEM systems as a first step toward the application of 3D-printed electronics.

RESULTS AND DISCUSSION

Fused deposition modeling (FDM), which is commonly used as the printing method in 3D printers, allows for the fabrication of parts using a range of materials, including elastomers and polymers.³⁵ FDM is an additive manufacturing technology through which thermoplastic materials are melted by a heating coil in an extruder, are laminated layer by layer, and are

hardened by a fan operating on each side of the work area to produce tangible objects. Thermoplastic materials suited to FDM-based 3D printers^{4,11,12,34,36} (CPLA (Proto-Plant Inc.) and PVA (eSUN Inc.)) were used in this study for the efficient fabrication of our 3D-printed MEM switches. Using an FDM-based 3D printer that is readily commercially available, we demonstrated the fabrication of two-terminal MEM switches (for information on the main components of the FDM-based 3D printer used in this study, see Figure S1 in Supporting Information). Figure 1a schematically illustrates the operating principle of our 3D-printed MEM switch design. The two-terminal MEM switch consists of a fixed bottom electrode and a freely suspended electrode with a hammerhead structure. When the switch is in the off state, an air gap separates the upper and lower electrodes such that ideally no current can flow between them. This is the main advantage of MEM switches, and indeed the only leakage current was found at the noise floor of our measurement setup. When a suitably large voltage difference is found between the electrodes, the suspended upper electrode is electrostatically actuated downward into contact with the fixed bottom electrode, generating a current path and causing the switch to enter the on state. This phenomenon is referred to as “pull-in”, and the voltage (V_{PI}) at which it occurs is dependent on design parameters of the switch used:^{27,37,38}

$$V_{PI} = \sqrt{\frac{8k_{eff}g_{air}^3}{27\epsilon_0 A_{overlap}}} \quad (1)$$

where k_{eff} is the effective spring constant of the suspended upper electrode, g_{air} is the as-fabricated air gap thickness, ϵ_0 is the permittivity of the vacuum, and $A_{overlap}$ is the overlapping area between the upper and lower electrodes. Notably, all of the materials used to fabricate our MEM switches were simultaneously printed by the 3D printer, facilitating easier fabrication compared to that achieved using the conventional manufacturing technique based on 2D processes. The design of the air gap is particularly important for determining the operation characteristics of a MEM switch; in our study, the air gap was easily formed by 3D printing a sacrificial layer and then dissolving it in water.

Figure 1b illustrates the fabrication process used for a 3D-printed two-terminal MEM switch. A 3D printer can control the density of printed material during printing. For this fabrication process, we selected a CPLA density value of 100% to enhance surface properties when the two electrodes were in contact with one another (see Figure S2 in Supporting Information). First, the nozzle temperature inside the 3D printer was set to 240 °C, which is the melting point of CPLA. A 300- μm -thick layer of CPLA was printed on a test printed circuit board (PCB) substrate to serve as the fixed bottom electrode. Then, a layer of PVA, which is soluble in water, was printed as a sacrificial layer at a nozzle temperature of 190 °C. Considering the length of the suspended electrode (L_{se}) that was to be printed later, the thickness of the PVA was designed to form a suitable air gap between the suspended upper electrode and the fixed bottom electrode. MEM switches require exerting very good control over g_{air} to minimize variations in operation characteristics; we achieved this by applying a PVA density level of 100%. Next, the freely suspended upper electrode was printed on the sacrificial PVA layer via CPLA. While printing the freely suspended electrode, we created a “hammerhead” structure at the end of the electrode to reduce V_{PI} by increasing A_{overlap} . In addition, V_{PI} can be further reduced by decreasing k_{eff} , which is expressed as follows (for more information on the derivation of k_{eff} see the Supporting Information):³⁹

$$k_{\text{eff}} = \frac{EW_1 t_{\text{se}}^3}{4L_{\text{se}}^3} \left(\frac{41(L_{\text{se}} - x)}{3L_{\text{se}} + 49.5x - 74.25x\left(\frac{x}{L_{\text{se}}}\right) + 29x\left(\frac{x}{L_{\text{se}}}\right)^2 - 7.25x\left(\frac{x}{L_{\text{se}}}\right)^3} \right) \quad (2)$$

where E is the Young's modulus for the upper electrode, W_1 is the width of the suspended upper electrode, and t_{se} is the printed thickness of the suspended upper electrode. Therefore, an increase in the distance (x) between the fixed bottom electrode and the anchor supporting the suspended electrode will result in a reduction in k_{eff} and in a corresponding decrease in V_{PI} (see Figure S3 in Supporting Information). For this calculation, we used an E value of 2465 ± 500 MPa, which was extracted from several CPLA samples using the American standard test method (see Figure S4 in Supporting Information). Additionally, it is important to optimize the thickness of the upper electrode because this value determines k_{eff} ; an excessively thin beam will collapse upon release due to stiction, whereas a thicker beam will have a higher V_{PI} value and hence will exhibit higher levels of dynamic power consumption. Thus, we applied a thickness of 360 μm , which is the lowest thickness that can support the freely suspended electrode during the release of the PVA sacrificial layer. As a final step, the manufactured device was immersed in deionized (DI) water and was subjected to ultrasonic treatment for a few minutes at room temperature to selectively dissolve the printed sacrificial PVA layer to form an air gap. We verified that structural and electrical properties of the CPLA remained unchanged while the CPLA was immersed in DI water (see Figures S5 and S6 in Supporting Information). In summary, using only a 3D printer, we fabricated our 3D-printed MEM switches without applying any complex processes (e.g., etching, annealing, or sintering). Although our MEM switches are larger in size than previously

reported MEM switches fabricated via conventional 2D processes, our devices can be scaled down using a state-of-the-art 3D printer.⁴⁰ Moreover, the entire process was performed at room temperature, and no high-temperature annealing or treatment was required; consequently, these devices are attractive for fabrication on a wide range of substrates. Figure 2a shows an optical image of a 3D-printed

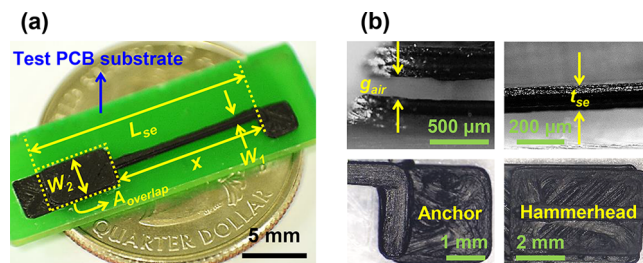


Figure 2. (a) A 3D-printed two-terminal MEM switch with a freely suspended electrode fabricated on a PCB substrate. (b) Magnified views of key components of the 3D-printed MEM switch: the g_{air} after the removal of the sacrificial PVA layer, the thickness t_{se} of the suspended electrode, the anchor supporting the suspended electrode, and the hammerhead structure of the suspended electrode.

two-terminal MEM switch. Magnified views of critical components of our MEM switch are shown in Figure 2b. Main parameters of the fabricated switch are illustrated in Table 1. After the removal of the sacrificial layer, the g_{air} between the

Table 1. Summary of the Parameters of the Fabricated MEM Switch

parameter	value
length of suspended top electrode (L_{se})	22 \pm 0.14 mm
width of suspended top electrode (W_1)	0.8 \pm 0.06 mm
width of hammerhead section of top electrode (W_2)	4.1 \pm 0.1 mm
distance between fixed bottom electrode and anchor (x)	1.6 \pm 0.17 mm
air gap thickness (g_{air})	0.12–0.19 mm
overlap area between top and bottom electrodes (A_{overlap})	24 \pm 0.91 mm ²
thickness of suspended top electrode (t_{se})	0.36 \pm 0.01 mm

two electrodes was evaluated through a microscope. The value of g_{air} was approximately 160 μm , which is significantly larger than the gaps of conventional MEM switches reported to date. However, the feasible gap size can be reduced using a state-of-the-art 3D printer. Furthermore, although we used a sequential two-step process in this study to form an air gap (i.e., first printing and then dissolving the sacrificial PVA layer), we also expect to be able to achieve necessary levels of mechanical separation in one step when using a high-performance 3D printer.

Figure 3a shows microscopic images of a 3D-printed MEM switch in the nonconducting and conducting states (i.e., the off and on states). In the off state, there is physical separation between the two electrodes that ensures the achievement of the off state. In the on state, the hammerhead region of the suspended electrode is in close contact with the bottom electrode, generating a current path. Electrical characteristics of the fabricated device are presented in Figure 3b. The voltage plotted on the x -axis is the voltage (V) applied between the upper and lower electrodes, and the current plotted on the y -axis is the current (I) flowing between the two electrodes. In the off state, the leakage current is immeasurably low (below

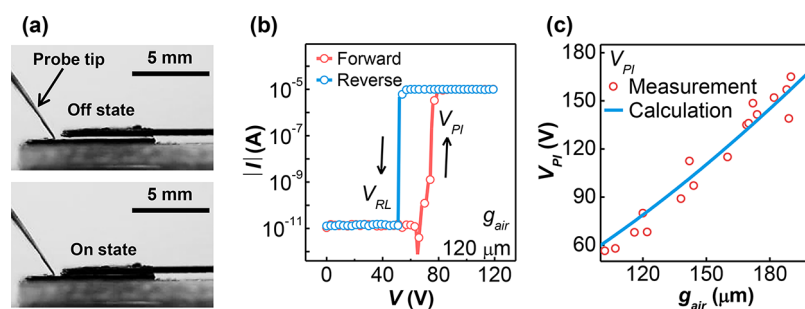


Figure 3. (a) Microscopic images of a 3D-printed MEM switch in the on and off states. (b) Measured I – V characteristics of the 3D-printed MEM switch. I was artificially limited to $10 \mu\text{A}$ to prevent significant Joule heating and consequent welding. (c) Comparison of the measured V_{PI} values for several 3D-printed MEM switches with different g_{air} values to the theoretically predicted values.

the noise floor of the parameter analyzer). As the voltage increases to above V_{PI} , the switch turns on, and the current rises quickly from the nonconducting off state to the conducting on state. The on/off current ratio exceeds 10^6 . The device shows abrupt switching characteristics: the subthreshold slope is less than 10 mV/dec , which is far lower than the theoretical limit (60 mV/dec) for CMOS devices at room temperature. When V is reduced to below the release voltage (V_{RL}), the 3D-printed MEM switch turns off because the sum of the electrostatic force and the surface adhesion force becomes lower than the spring restoring force.

The V_{PI} of an MEM switch is the most important indicator of device performance; hence, we compared the measured V_{PI} values with the calculated values as a function of g_{air} , as shown in Figure 3c. The symbols shown correspond to sets of measured V_{PI} values for 3D-printed MEM switches with various gap sizes g_{air} and the lines represent theoretically predicted values calculated from the simplified model of a two-terminal MEM switch (eq 1). For this calculation, we used a k_{eff} value of 2.73 N/m obtained from eq 2 by considering the structure of our switches. Although some discrepancy between the calculated and measured values can be observed because of the nonuniform thickness that arose during layer-by-layer stacking when printing the PVA layer, we found an effective reduction in V_{PI} with a decreasing g_{air} . This consistency between the measured and calculated values shows that the simplified model is well suited to describe the electro-mechanical behaviors of our 3D-printed MEM switches, facilitating design-to-fabrication consistency. In addition, a further reduction in V_{PI} is expected to be achieved by more accurately controlling the thickness of the printed PVA layer.

Representative I – V characteristics of a 3D-printed MEM switch with a g_{air} of $190 \mu\text{m}$ as observed during cyclic measurements are shown in Figure 4. The I – V curves, which rose at slightly varying values of V_{PI} during cyclic testing, show the occurrence of mechanical actuation induced by the electrostatic force. In the first two cycles, I rose at the same V_{PI} , but after these two cycles, the V_{PI} value suddenly decreased, indicating a change in g_{air} and a physical degradation of the contact surface.^{41,42} As the thermoplastic material (i.e., CPLA) used to fabricate the electrodes has a lower melting point and is softer than typical metals, the 3D-printed MEM switch underwent unwanted V_{PI} degradation. Although the device showed poor levels of reliability, it is encouraging to note that the introduction of harder 3D-printable metals with better resistance to corrosion and contamination compared to CPLA can lead to further improvements in the reliability of 3D-printed materials.

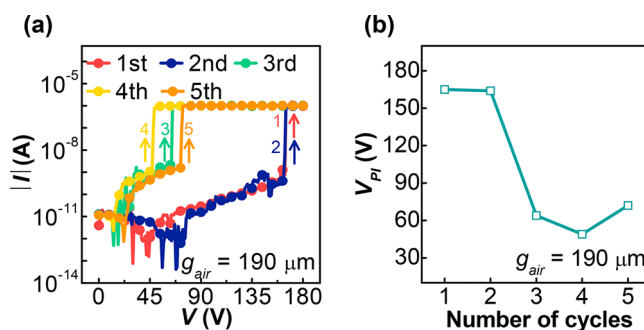


Figure 4. (a) Representative I – V characteristics of a 3D-printed MEM switch with a g_{air} of $190 \mu\text{m}$ during cyclic measurements. (b) V_{PI} values extracted from the cyclic measurements. The value of V_{PI} decreased as the number of contact instances increased because of the physical degradation of the contact surface.

CONCLUSION

We have demonstrated the facile fabrication of two-terminal MEM switches using a commercially available FDM-based 3D printer. We fabricated MEM switches in a single printing step using 3D-printable thermoplastic materials. Our 3D-printed MEM switch design has a two-terminal structure with a freely suspended upper electrode and a fixed lower electrode printed from CPLA. In addition, to achieve the physical separation of the two electrodes, a layer of water-soluble PVA was printed between the electrodes. Our 3D-printed MEM switches exhibit excellent electromechanical properties in both the on and off states, showing promise for the applicability of 3D-printed electronic devices. Consequently, 3D-printed MEM switches are intriguing candidates for the implementation of high-throughput and low-cost MEM devices.

METHODS

The 3D printing process was performed using a SPROUT single-nozzle 3D printer (Former's Farm, Inc., Korea). Using only a CAD file, we fabricated 3D-printed MEM switches by loading the CAD file to the 3D printer software program. The designed MEM switches were printed layer by layer. In our experiment, the diameter of the 3D printing nozzle was set to $400 \mu\text{m}$, and the nozzle moved at a speed of 10 mm/s . For CPLA and PVA printing, nozzle temperatures were set to 240 and $190 \text{ }^\circ\text{C}$, respectively, which are close to the melting points of each material. The process of fabricating an entire MEM switch took less than 30 min , including the 3D printing process required to produce electrodes and the sacrificial layer and the process of dissolving the sacrificial layer to form an air gap.

■ ASSOCIATED CONTENT

● Supporting Information

The Supporting Information is available free of charge on the ACS Publications website at DOI: 10.1021/acsami.8b01455.

Additional information on the main components of the FDM-based 3D printer, top-view micrograph images of the CPLA with various densities, derivations of the k_{eff} equation, calculations of the normalized k_{eff} values with increasing x , the calculation of the Young's modulus for the 3D-printed CPLA, experiments on the selectivity of the PVA sacrificial layer, and the measurement of the resistivity of CPLA using the Van der Pauw method (PDF)

■ AUTHOR INFORMATION

Corresponding Authors

*E-mail: sjchoiee@kookmin.ac.kr.

*E-mail: sungho85kim@sejong.ac.kr.

ORCID

Sung-Jin Choi: 0000-0003-1301-2847

Author Contributions

[#]These authors (Y.L. and J.H.) equally contributed to this work.

Notes

The authors declare no competing financial interest.

■ ACKNOWLEDGMENTS

This work was supported by the National Research Foundation (NRF) of Korea under Grants 2016R1A2B4011366 and 2016R1A5A1012966 and through the Future Semiconductor Device Technology Development Program (Grant 10067739) funded by MOTIE (Ministry of Trade, Industry & Energy) and KSRC (Korea Semiconductor Research Consortium).

■ REFERENCES

- (1) Goyanes, A.; Wang, J.; Buanz, A.; Martínez-Pacheco, R.; Telford, R.; Gaisford, S.; Basit, A. W. 3D Printing of Medicines: Engineering Novel Oral Devices with Unique Design and Drug Release Characteristics. *Mol. Pharmaceutics* **2015**, *12*, 4077–4084.
- (2) Farahani, R. D.; Dubé, M.; Theriault, D. Three-Dimensional Printing of Multifunctional Nanocomposites: Manufacturing Techniques and Applications. *Adv. Mater.* **2016**, *28*, 5794–5821.
- (3) Gross, B. C.; Erkal, J. L.; Lockwood, S. Y.; Chen, C.; Spence, D. M. Evaluation of 3D Printing and Its Potential Impact on Biotechnology and the Chemical Sciences. *Anal. Chem.* **2014**, *86*, 3240–3253.
- (4) Leigh, S. J.; Bradley, R. J.; Purcell, C. P.; Billson, D. R.; Hutchins, D. A. A Simple, Low-Cost Conductive Composite Material for 3D Printing of Electronic Sensors. *PLoS One* **2012**, *7*, e49365.
- (5) Derby, B. Printing and Prototyping of Tissues and Scaffolds. *Science* **2012**, *338*, 921–926.
- (6) Espalin, D.; Muse, D. W.; MacDonald, E.; Wicker, R. B. 3D Printing Multifunctionality: Structures with Electronics. *Int. J. Adv. Manuf. Technol.* **2014**, *72*, 963–978.
- (7) Wong, J. Y.; Pfahnl, A. C. 3D Printing of Surgical Instruments for Long-Duration Space Missions. *Aviat., Space Environ. Med.* **2014**, *85*, 758–763.
- (8) Zhang, Q.; Zhang, F.; Medarametla, S. P.; Li, H.; Zhou, C.; Lin, D. 3D Printing of Graphene Aerogels. *Small* **2016**, *12*, 1702–1708.
- (9) Ladd, C.; So, J.-H.; Muth, J.; Dickey, M. D. 3D Printing of Free Standing Liquid Metal Microstructures. *Adv. Mater.* **2013**, *25*, 5081–5085.
- (10) Seitz, H.; Rieder, W.; Irsen, S.; Leukers, B.; Tille, C. Three-Dimensional Printing of Porous Ceramic Scaffolds for Bone Tissue Engineering. *J. Biomed. Mater. Res., Part B* **2005**, *74B*, 782–788.
- (11) Ambrosi, A.; Pumera, M. Self-Contained Polymer/Metal 3D Printed Electrochemical Platform for Tailored Water Splitting. *Adv. Funct. Mater.* **2017**, *1700655*, 1700655.
- (12) Chen, H.; Yang, X.; Chen, L.; Wang, Y.; Sun, Y. Application of FDM Three-Dimensional Printing Technology in the Digital Manufacture of Custom Edentulous Mandible Trays. *Sci. Rep.* **2016**, *6*, 19207.
- (13) Taboas, J.; Maddox, R.; Krebsbach, P.; Hollister, S. Indirect Solid Free Form Fabrication of Local and Global Porous, Biomimetic and Composite 3D Polymer-Ceramic Scaffolds. *Biomaterials* **2003**, *24*, 181–194.
- (14) Carrico, J. D.; Traeden, N. W.; Aureli, M.; Leang, K. K. Fused Filament 3D Printing of Ionic Polymer-Metal Composites (IPMCs). *Smart Mater. Struct.* **2015**, *24*, 125021.
- (15) Lam, C. X.; Mo, X.; Teoh, S.; Hutmacher, D. W. Scaffold Development Using 3D Printing with a Starch-Based Polymer. *Mater. Sci. Eng., C* **2002**, *20*, 49–56.
- (16) Kong, Y. L.; Tamargo, I. A.; Kim, H.; Johnson, B. N.; Gupta, M. K.; Koh, T. W.; Chin, H. A.; Steingart, D. A.; Rand, B. P.; McAlpine, M. C. 3D Printed Quantum Dot Light-Emitting Diodes. *Nano Lett.* **2014**, *14*, 7017–7023.
- (17) Fu, K.; Wang, Y.; Yan, C.; Yao, Y.; Chen, Y.; Dai, J.; Lacey, S.; Wang, Y.; Wan, J.; Li, T.; Wang, Z.; Xu, Y.; Hu, L. Graphene Oxide-Based Electrode Inks for 3D-Printed Lithium-Ion Batteries. *Adv. Mater.* **2016**, *28*, 2587–2594.
- (18) Lewis, J. A.; Ahn, B. Y. Three-dimensional printed electronics. *Nature* **2015**, *518*, 42–43.
- (19) Fu, K.; Yao, Y.; Dai, J.; Hu, L. Progress in 3D Printing of Carbon Materials for Energy-Related Applications. *Adv. Mater.* **2017**, *29*, 1603486.
- (20) Abele, N.; Fritschi, R.; Boucart, K.; Casset, F.; Ancey, P.; Ionescu, A. M. Suspended-Gate MOSFET: Bringing New MEMS Functionality into Solid-State MOS Transistor. *IEEE IEDM Technical Digest* **2005**, *1*, 479–481.
- (21) Otis, B. P.; Chee, Y. H.; Lu, R.; Pletcher, N. M.; Rabaey, J. M. An Ultra-Low Power MEMS-Based Two-Channel Transceiver for Wireless Sensor Networks. *IEEE Symposium on VLSI Technology* **2004**, *1*, 20–23.
- (22) Sekitani, T.; Takamiya, M.; Noguchi, Y.; Nakano, S.; Kato, Y.; Sakurai, T.; Someya, T. A Large-Area Wireless Power-Transmission Sheet using Printed Organic Transistors and Plastic MEMS switches. *Nat. Mater.* **2007**, *6*, 413–417.
- (23) Lee, K.-W.; Noriki, A.; Kiyoyama, K.; Fukushima, T.; Tanaka, T.; Koyanagi, M. Three-Dimensional Hybrid Integration Technology of CMOS, MEMS, and Photonics Circuits for Optoelectronic Heterogeneous Integrated Systems. *IEEE Trans. Electron Devices* **2011**, *58*, 748–757.
- (24) Osoba, B.; Saha, B.; Dougherty, L.; Edgington, J.; Qian, C.; Niroui, F.; Lang, J. H.; Bulovic, V.; Wu, J.; Liu, T.-J. K. Sub-50 mV NEM Relay Operation Enabled by Self-Assembled Molecular Coating. *IEEE IEDM Technical Digest* **2016**, *1*, 26.8.1.
- (25) Brown, E. R. RF-MEMS Switches for Reconfigurable Integrated Circuits. *IEEE Trans. Microwave Theory Tech.* **1998**, *46*, 1868–1880.
- (26) Rebeiz, G. M. RF MEMS Switches: Status of the Technology. *Proc. 12th Int. Conf. Transducers, Solid-State Sens. Actuators Microsyst.* **2003**, *2*, 1726–1729.
- (27) Kim, H. C.; Chun, K. RF MEMS Technology. *IEEJ Trans. Electr. Electron. Eng.* **2007**, *2*, 249–261.
- (28) Chung, S.; Ul Karim, M. A.; Kwon, H.-J.; Subramanian, V. High-Performance Inkjet-Printed Four-Terminal Microelectromechanical Relays and Inverters. *Nano Lett.* **2015**, *15*, 3261–3266.
- (29) Park, E. S.; Chen, Y.; Liu, T. K.; Subramanian, V. Inkjet-Printed Micro-Electro-Mechanical Switches. *IEEE IEDM Technical Digest* **2011**, *1*, 29.2.1.
- (30) Park, E. S.; Chen, Y.; Liu, T.-J. K.; Subramanian, V. A New Switching Device for Printed Electronics: Inkjet-Printed Microelectromechanical Relay. *Nano Lett.* **2013**, *13*, 5355–5360.
- (31) Mohanty, S.; Larsen, L. B.; Trifol, J.; Szabo, P.; Burri, H. V. R.; Canali, C.; Dufva, M.; Emnéus, J.; Wolff, A. Fabrication of Scalable and

Structured Tissue Engineering Scaffolds Using Water Dissolvable Sacrificial 3D Printed Moulds. *Mater. Sci. Eng., C* **2015**, *55*, 569–578.

(32) Jin, S. H.; Shin, J.; Cho, I.-T.; Han, S. Y.; Lee, D. J.; Lee, C. H.; Lee, J.-H.; Rogers, J. A. Solution-Processed Single-Walled Carbon Nanotube Field Effect Transistors and Bootstrapped Inverters for Disintegratable, Transient Electronics. *Appl. Phys. Lett.* **2014**, *105*, 13506.

(33) Goyanes, A.; Robles Martinez, P.; Buanz, A.; Basit, A. W.; Gaisford, S. Effect of Geometry on Drug Release from 3D Printed Tablets. *Int. J. Pharm.* **2015**, *494*, 657–663.

(34) Goyanes, A.; Buanz, A. B. M.; Basit, A. W.; Gaisford, S. Fused-Filament 3D Printing (3DP) for Fabrication of Tablets. *Int. J. Pharm.* **2014**, *476*, 88–92.

(35) Dudek, P. FDM 3D Printing Technology in Manufacturing Composite Elements. *Arch. Metall. Mater.* **2013**, *58*, 1415–1418.

(36) Li, X.; Kanjwal, M. A.; Lin, L.; Chronakis, I. S. Electrospun Polyvinyl-Alcohol Nanofibers as Oral Fast-Dissolving Delivery System of Caffeine and Riboflavin. *Colloids Surf., B* **2013**, *103*, 182–188.

(37) Rebeiz, G. M.; Muldavin, J. B. RF MEMS Switches and Switch Circuits. *IEEE Microw. Mag.* **2001**, *2*, 59–71.

(38) Rebeiz, G. M. *RF MEMS Theory, Design, and Technology*; John Wiley & Sons, Inc.: Hoboken, NJ, 2003; Chapter 2, pp 36–38.

(39) Saha, S. C.; Hanke, U.; Jensen, G. U.; Sæther, T. Modeling of Spring Constant and Pull-down Voltage of Non Uniform RF MEMS Cantilever. In *IEEE Proceedings of Behavioral Modeling and Simulation Workshop*; IEEE: New York, 2006; pp 56–60.

(40) Chung, M.; Radacsi, N.; Robert, C.; McCarthy, E. D.; Callanan, A.; Conlisk, N.; Hoskins, P. R.; Koutsos, V. On the Optimization of Low-Cost FDM 3D Printers for Accurate Replication of Patient-Specific Abdominal Aortic Aneurysm Geometry. *3D Print. Med.* **2018**, *4*, 2–10.

(41) McGruer, N. E.; Adams, G. G.; Chen, L.; Guo, Z. J.; Du, Y. Mechanical, Thermal, and Material Influences on Ohmic-Contact-Type MEMS Switch Operation. In *IEEE 19th International Microelectromechanical Systems Conference*; IEEE: New York, 2006; pp 230–233.

(42) Yi, Z.; Guo, J.; Chen, Y.; Zhang, H.; Zhang, S.; Xu, G.; Yu, M.; Cui, P. Vertical, Capacitive Microelectromechanical Switches Produced Via Direct Writing of Copper Wires. *Microsyst. Nanoeng.* **2016**, *2*, 16010.

Supporting Information for

Three-Dimensionally Printed Microelectromechanical Switches

Yongwoo Lee^{1,†}, Jungmin Han^{1,†}, Bongsik Choi¹, Jinsu Yoon¹, Jinhee Park¹, Yeamin Kim¹, Jieun Lee¹,
Dae Hwan Kim¹, Dong Myong Kim¹, Meehyun Lim², Min-Ho Kang³, Sungho Kim^{4,*},
and Sung-Jin Choi^{1,*}

¹School of Electrical Engineering, Kookmin University, Seoul 02707, Korea

²Mechatronics R&D Center, Samsung Electronics, Gyeonggi-do 18448, Korea

³Department of Nano-process, National Nanofab Center (NNFC), Daejeon 34141, Korea

⁴Department of Electrical Engineering, Sejong University, Seoul 05006, Korea

Email: sjchoiee@kookmin.ac.kr and sungho85kim@sejong.ac.kr

[†]These authors equally contributed to this work.

S1. Main components of the FDM-based 3D printer

Figure S1 shows photographic images of the 3D printer, which operates based on the FDM method, and the main components of the 3D printer, including the bed, fans, and extruder. Thermoplastic material is printed on the bed at a controlled temperature. The bed can move semi-automatically in the vertical direction, and care must be taken to properly adjust the printing position. A fan is located on each side of the extruder to cool the printed thermoplastic to quickly to solidify it. As a component of the extruder, the heating coil melts the thermoplastic by heating it to a temperature exceeding its melting point. As another component of the extruder, the nozzle can withstand temperatures exceeding the melting points of 3D-printable thermoplastics, as it is composed of stainless steel with low thermal conductivity.

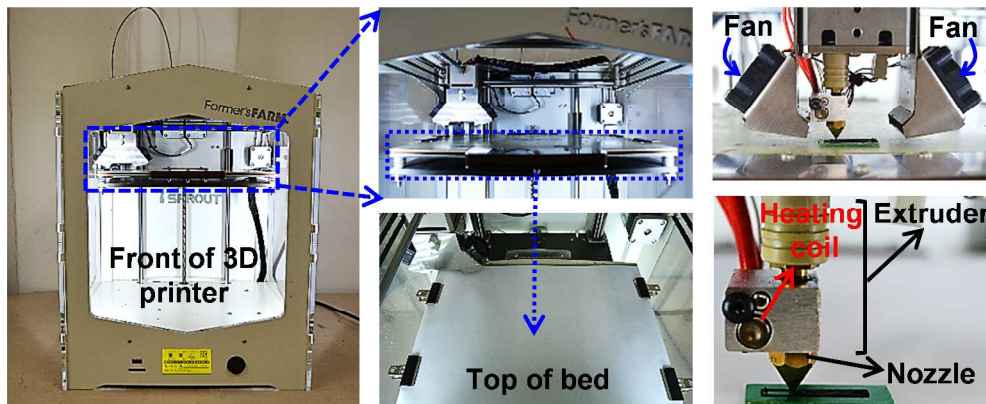


Figure S1. Photographs of the FDM-based 3D printer used to fabricate the 3D-printed MEM switches and its components.

S2. Top-view micrograph images of the 3D-printed CPLA of various densities

Figure S2 shows top-view micrograph images of the 3D-printed CPLA layers of various densities (25%, 50%, 75%, and 100%). The internal density of the printed structures can easily be controlled using a 3D printer; hence, a higher density can generate enhanced surface properties in the printed structures. As the two electrodes are in contact with one another in an on state in our 3D-printed MEM switches, it is necessary to print the CPLA at a density of 100% to improve surface characteristics.

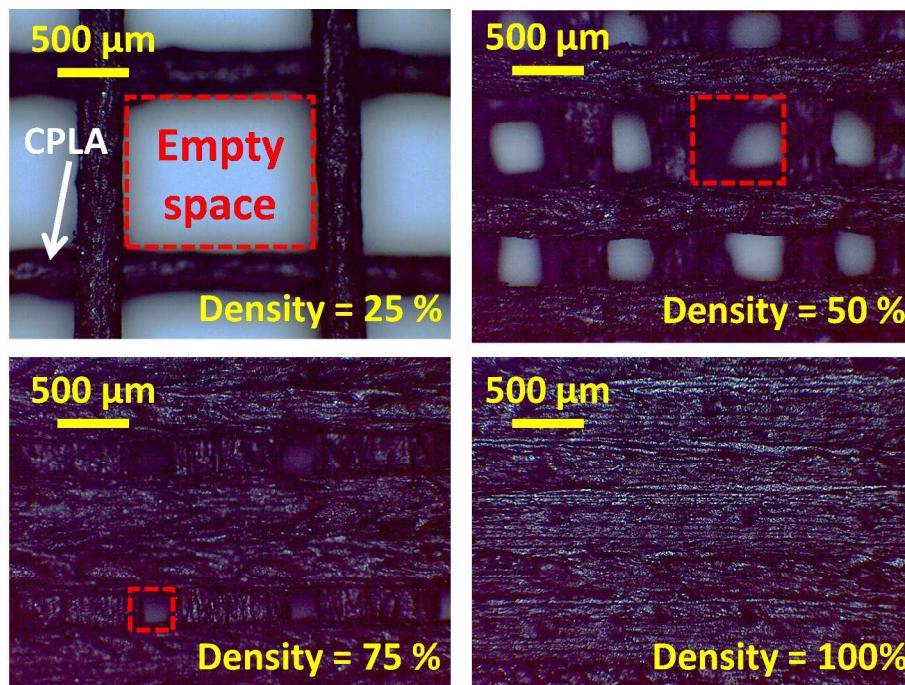


Figure S2. Micrograph images of the 3D-printed CPLA layers of various densities (25%, 50%, 75%, and 100%).

S3. Derivations of the k_{eff} equation and calculations of the normalized k_{eff} values for the two-terminal MEM switches

In our previous study, the k_{eff} for two-terminal MEM switches with a hammerhead structure is denoted by the following equation:

$$k_{eff} = \frac{24EI_m y}{3(L_{se} - x)(L_{se} + x)^2 + 2yx^2(x + 3L_{se}) + 12xL_{se}(L_{se} - x)(y - 1)} \quad (S1)$$

where I_m is the moment of inertia of the suspended electrode and y is a constant value that divides the W_2 of 4.1 mm by the W_1 of 0.8 mm. Here, I_m is defined by solving the following:

$$I_m = \frac{W_1 t_{se}^3}{12} \quad (S2)$$

Therefore, by rearranging the y value (5.125) and by adding Eq. S2 to Eq S1, the modified k_{eff} equation can be expressed.

Moreover, to investigate the effect of x on k_{eff} , we calculated normalized k_{eff} values as a function of x . Figure S3a presents a schematic illustration of MEM switches with increasing x values; Figure S3b shows the normalized k_{eff} results. As x increases, k_{eff} ultimately reaches a negative value. The k_{eff} values were normalized with respect to the value corresponding to $x = 0$.

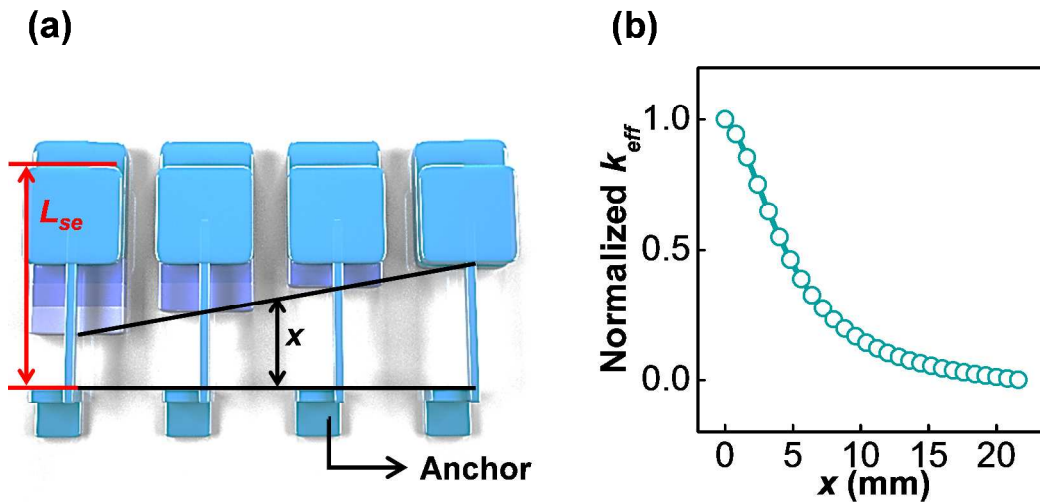


Figure S3. (a) Schematic illustration of 3D-printed MEM switches with increasing x values. (b) Calculated normalized k_{eff} values for different x values.

S4. Calculation of the Young's modulus for the 3D-printed CPLA

To examine the mechanical properties of the printed CPLA, we measured the Young's modulus (E) of several CPLA samples using the American standard test method (ASTM) D638. Samples of a predetermined standard size were printed, and E was then measured for each sample by analysing the measured stress relative to the applied strain at a strain rate of 9.75 mm/sec as shown in Figure S4a. The value of E can be extracted from the initial slope of the stress-strain curve and thus it can be expressed as the following equation:

$$E = \left. \frac{d(\text{stress})}{d(\Delta L/L_0)} \right|_{\Delta L/L_0=0} \quad (\text{S3})$$

where L_0 is the initial length of the sample and ΔL is the stretched length of the sample. We measured the stress-strain curves of six CPLA samples. The average E value of the samples was found to be approximately $2465 \text{ MPa} \pm 500 \text{ MPa}$ as shown in Figure S4b and Figure S4c. Notably, we printed the CPLA 100% density when fabricating the 3D-printed MEM switches; however, CPLA density can be controlled during 3D printing, suggesting that the E value can be adjusted by varying the density level. This density dependence of the mechanical properties of 3D-printed materials is expected to afford 3D-printed MEM switches additional design versatility; density levels can be adjusted to tune E , which in turn determines the k_{eff} value of the suspended CPLA electrode.

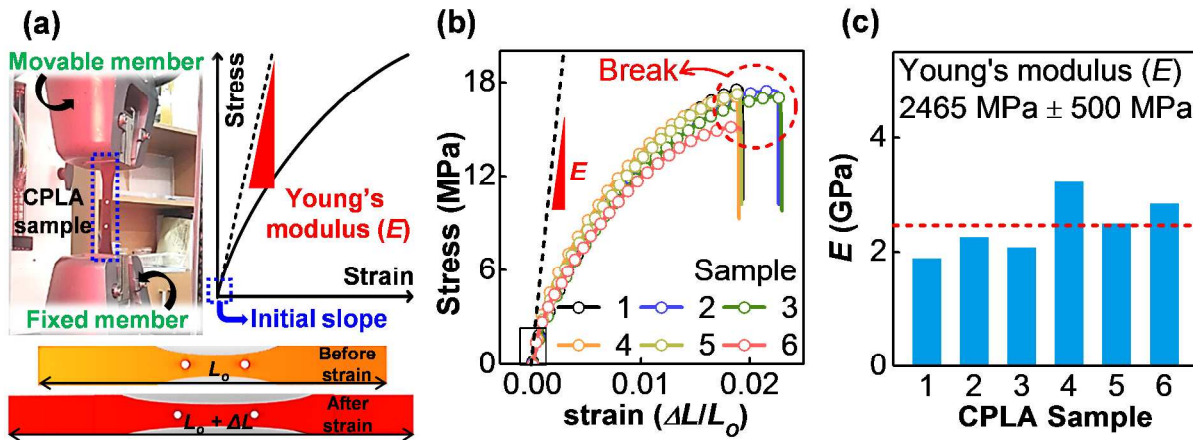


Figure S4. (a) Procedure for measuring E values of the printed CPLA samples. The values of E were extracted from the measured stress-strain curves. (b) The stress-strain curves from which the E values were extracted. (c) The E values extracted from the six samples.

S5. Selectivity and volume change of the sacrificial PVA layer in water

To confirm the selectivity and volume change behaviours of the PVA in DI water, we immersed a 3D-printed PVA layer printed on a CPLA layer with dimensions of 10 mm × 10 mm × 0.5 mm in DI water. As shown in Figure S5a, the printed PVA layer dissolved fully within a few minutes. After dissolving the PVA layer in DI water, we found no deformation of or damage to the CPLA. No significant volume changes were observed when comparing volumes of the CPLA before and after PVA dissolution, as shown in Figure S5b.

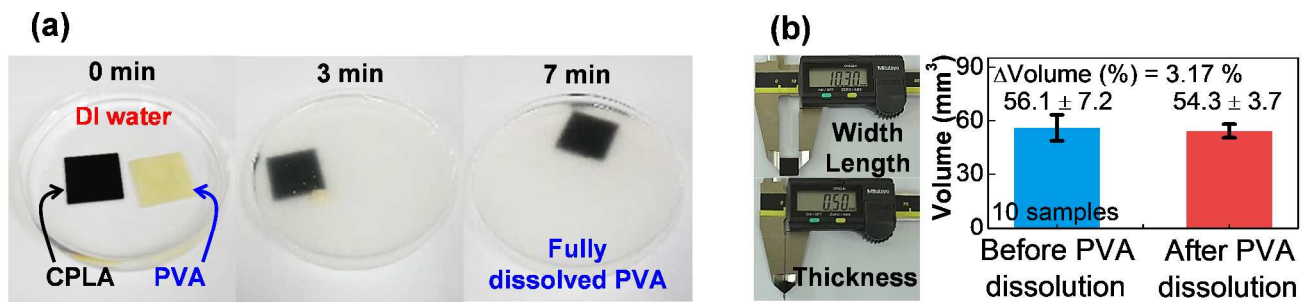


Figure S5. (a) Dissolution of a 3D-printed PVA layer in DI water. (b) Volume change of the CPLA sample before and after PVA dissolution.

S6. Measurement of the resistivity of CPLA using the Van der Pauw method.

To investigate the electrical properties of CPLA, we measured CPLA resistivity using the Van der Pauw method. The Van der Pauw method can be used to accurately measure the characteristics of any arbitrary shape so long as the sample is approximately two-dimensional and solid and has electrodes in place. First, one can flow the current along one edge of the sample and measure the voltage across the opposite edge. Further, by changing the direction of the current and by measuring the voltage, two voltage drop values can be obtained. By measuring the voltage by shifting the electrode in the clockwise direction as shown in Figure S6a, the electrical resistivity (ρ) of CPLA can be derived from a total of eight voltage drop values. ρ is expressed by the following equation:^{S1}

$$\rho_A = \frac{\pi}{\ln 2} f_A t_{CPLA} \frac{(V_1 - V_2 + V_3 - V_4)}{4I} \quad (S4)$$

$$\rho_B = \frac{\pi}{\ln 2} f_B t_{CPLA} \frac{(V_5 - V_6 + V_7 - V_8)}{4I} \quad (S5)$$

$$\rho = \frac{\rho_A + \rho_B}{2} \quad (S6)$$

where f_A and f_B are geometric factors based on sample symmetry, t_{CPLA} is the thickness of the CPLA sample, V_1 - V_8 denote measured voltages, and I is the current injected through the CPLA sample. f_A and f_B can be extracted from Eq. S7 and Eq. S8, respectively, as follows:

$$\frac{Q_A - 1}{Q_A + 1} = \frac{f_A}{\ln 2} \operatorname{arccosh} \left(\frac{e^{\ln 2 / f_A}}{2} \right) \quad (S7)$$

$$\frac{Q_B - 1}{Q_B + 1} = \frac{f_B}{\ln 2} \operatorname{arccosh} \left(\frac{e^{\ln 2 / f_B}}{2} \right)$$

(S8)

where Q_A and Q_B are the ratio of the resistance measured from the length and width directions of the CPLA sample. Q_A and Q_B are calculated as follows:

$$Q_A = \frac{V_1 - V_2}{V_3 - V_4} \quad (S9)$$

$$Q_B = \frac{V_5 - V_6}{V_8 - V_7} \quad (\text{S10})$$

We calculate Q_A and Q_B from Eq. S9 and Eq. S10, respectively, with the measured voltage values and substitute them into Eq. S7 and Eq. S8 to derive f_A and f_B values by numerical calculation. Finally, we obtain ρ_A and ρ_B from Eq. S4 and Eq. S5 and we determine the ρ value for CPLA from Eq. S6.

Our printed CPLA sample size is $10 \text{ mm} \times 10 \text{ mm} \times 0.5 \text{ mm}$ and the actual measurement image is shown in Figure S6b. We confirm that printing and dissolving the sacrificial PVA layer did not significantly affect the ρ of CPLA by measuring ρ from the test thin-plate-like printed CPLA using the Van der Pauw method as shown in Figure S6c.

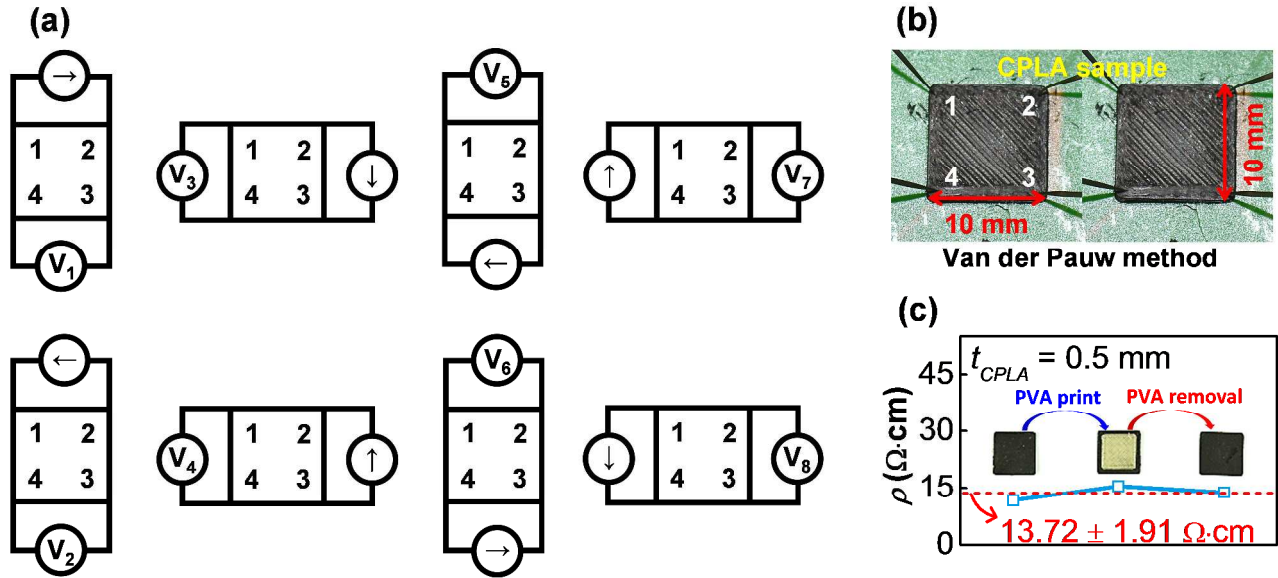


Figure S6. (a) The sequence of Van der Pauw method measurement procedures. (b) Images of the CPLA samples for measuring ρ via the Van der Pauw method. (c) ρ values extracted from printed CPLA, from CPLA after PVA printing on the CPLA, and from CPLA after the removal of PVA samples.

REFERENCES

- (S1) Ramadan, A. A.; Gould, R. D., Ashour, A. A. On the Van Der Pauw Method of Resistivity Measurements. *Thin Solid Films* **1994**, *239*, 272-275.